Int. J. Adhesion & Adhesives, 23, 2003, 293-305

MEASURING THE MODE I ADHESIVE FRACTURE ENERGY, G_{IC}, OF STRUCTURAL ADHESIVE JOINTS: THE RESULTS OF AN INTERNATIONAL ROUND-ROBIN.

B.R.K. BLACKMAN*, A.J. KINLOCH, M. PARASCHI AND W.S. TEO

Department of Mechanical Engineering, Imperial College London, South Kensington Campus, Exhibition Road, London SW7 2AZ. UK.

Abstract

The results of an inter-laboratory round-robin test programme designed to validate a new protocol for determining the mode I adhesive fracture energy, G_{IC}, of structural adhesive joints are presented. The analysis schemes employed by the protocol are described and critically compared in the light of these results. The importance of a number of validity checks on the data analyses are discussed and the accuracy and precision of the test method is determined according to existing International standards. The values of G_{IC} deduced were shown to be independent of the test geometry of the joint (i.e. DCB versus TDCB) but dependent upon the substrate material used. Additional studies have shown that the substrate dependence was due to the cured adhesive in the different joints possessing different values of glass transition temperature.

Keywords: A. Epoxy; B. Composites; C. Fracture mechanics; D. Fracture; Standardisation

1. Introduction

Fracture mechanics has become a very popular tool for the characterisation of adhesive joints in recent years. Fracture mechanics tests are routinely conducted by industry during materials development and have also found extensive application in fatigue and durability studies over the past twenty years [1]. More recently, fracture mechanics data has been used to predict the impact failure response of, for example, the impact wedge peel test [2] and currently fracture mechanics data are finding application in structural impact studies via the use of cohesive zone models [3, 4]. The use of Linear Elastic Fracture Mechanics (LEFM) tests to measure the mode I adhesive fracture energy, G_{IC}, of adhesive joints dates back to the work of Ripling and co-workers in the 1960s [5, 6] who developed a mode I test method to measure the

* Corresponding author. Tel.: +44 (0)20 7594 7196; fax: +44 (0)20 7594 7017
E-mail address: b.blackman@imperial.ac.uk

toughness of structural bonds between metallic substrates. This work led to the publication of an ASTM standard in 1973 [7]. Since then, the many developments in the application of fracture mechanics to, for example, fibre-reinforced polymer composites [8, 9] has created great potential for the development of a new test protocol for structural adhesive joints. It was against this background that a technical committee of the European Structural Integrity Society (ESIS) commenced work on structural adhesives test methods in 1997. Two of the present authors, who are members of the "ESIS Technical Committee 4 on Polymers Adhesives and Composites," drafted a new mode I test protocol [10] and launched an inter-laboratory round-robin test programme to evaluate the method and to determine its precision. The new protocol accommodated the use of both metallic and fibre reinforced polymer composite substrates. During the course of the wide ranging programme involving ten test laboratories, modifications were made to both the experimental and analytical procedures compared to the original ASTM standard of 1973. For example, a new corrected beam theory analysis for the tapered double cantilever beam was developed [11] and a correction for system compliance and additional validity checks were built into the experimental procedure. Following these modifications, the revised protocol was submitted to the British Standards Institution for consideration as a British Standard (under the direction of the "Adhesives Standards Policy Committee PRI/52") and was accepted and subsequently published in 2001 [12]. It is intended that this document should also be published as a European standard. The present work describes the stages in the development of the new protocol and the modifications made in the light of the results from the round-robin tests.

2. The inter-laboratory round-robin test programme

2.1. Introduction

Three different substrate materials were studied in the round-robin. These were a unidirectional carbon-fibre reinforced plastic (CFRP) IM7/977-2 from Cytec Fiberite, an aluminium alloy (grade BS EN 5083) and mild steel (grade EN24). These substrates were all bonded with the same general-purpose structural epoxy-paste adhesive to make either double cantilever beam (DCB) or tapered double cantilever beam (TDCB) test specimens as shown in Figure 1. The TDCB specimen was included because it is a very popular test specimen in adhesives research because the height taper: (i) allows substrate materials with a relatively low yield stress to be tested without plastic deformation of the substrate arms occurring and (ii) renders the rate of change of specimen compliance independent of crack length (see later).

2.2. Adhesive joint manufacture

All the adhesive joints tested in the round-robin were manufactured in a single laboratory by experienced personnel. The substrate materials were all stored in normal laboratory conditions prior to joint manufacture. Details of the dimensions of the joints manufactured are given in Table 1. All substrates were initially cleaned with a fresh cloth soaked in acetone. They were then abraded with 180/220 mesh alumina grit prior to final solvent cleaning with acetone. The mild steel substrates were additionally cleaned in a solvent degreaser containing 1,1,1 trichloro-ethylene both before and after grit blasting. Adhesive was applied to each substrate and evenly spread across the surface. To maintain the constant bond-line thickness, either glass balotini or steel wires of diameter 0.4mm were used. Balotini was used for the CFRP joints and was lightly scattered across the adhesive prior to forming the joint. The steel wires were used with the metallic substrates and were inserted into the ends of the bond-line prior to forming the joint. At this stage, a single 12.5μm thick film of PTFE was inserted at one end to act as a crack starter as specified in the protocol [10]. After the joints were formed they were placed in a bonding jig, the top plate of which was secured with bolts tightened to a torque of 4Nm. For each batch of joints manufactured, a thermocouple lead was inserted in to the bond-line of one joint to monitor the temperature during cure. The joint assembly was then placed in the oven to cure the adhesive. The adhesive manufacturer's cure cycle was followed closely. On removal from the oven, the joints were ejected from the jig and any excess adhesive was removed from the sides of the specimen.

2.3. The test matrix

Samples were sent to twelve laboratories, ten of which went on to participate in the round-robin. Laboratories 1-5 received four CFRP/DCB and four TDCB/Mild-steel joints. Laboratories 6-10 received four DCB/Mild-steel and four TDCB/Al-alloy joints.

2.4. The test procedure

The laboratories were asked to conduct the fracture tests according to the protocol [10]. This involved first preparing the specimens for testing by taking precise measurements of the specimens' dimensions and coating the side of the joint with a thin layer of white correction fluid or aqueous based paint so as to facilitate the crack length measurements. The specimens

had either been drilled with 8mm loading holes through the substrates, or had had load blocks bonded on (as shown in Figure 1). Hence, the participants were required to use equivalent diameter loading pins to couple the test specimen to the test frame. To make the total test duration approximately equivalent for all joints, the CFRP joints were to be tested at a constant cross-head displacement rate of 1mm/min, whilst all the remaining joints were to be tested at 0.1mm/min. The choice of crosshead speeds was determined by a consideration of both the different substrate modulus values and the different substrate heights, as outlined by Atkins and Mai [13]. Whilst the crack speed decreases in the DCB specimen as the crack grows [13], this was considered to have minimal influence on the measured values of G_{IC} because the epoxy adhesive used had a high T_g and a low degree of viscoelasticity [14]. The procedure followed was to initiate the crack firstly from the insert film and then from the resulting mode I precrack. Full specimen unloading would be carried out in between these two stages. When the crack re-initiated from the mode I precrack, crack propagation would be monitored such that a complete resistance curve (i.e. an "R-curve") could be drawn. After the crack had propagated approximately 80mm, the specimens were to be fully unloaded and any permanent offset displacement, termed δ_{offset}, on the loading trace was to be noted. This provided a visual indication of whether any permanent plastic deformation of the substrates had occurred during loading. Although it is normal for small final offsets to be observed on unloading because of the presence of the deformed adhesive slightly propping open the crack, experience has shown that if this is less than about 5% of the maximum opening displacement used in the test, then it is unlikely that plastic deformation of the substrates will have occurred.

Values of G_{IC} at crack initiation were measured for each joint from both the insert film and from a mode I pre-crack formed during the initial load-unload cycle. For consistency with the standard for composite delamination testing in mode I [9], crack initiation has been defined in three ways, i.e. (a) by a deviation from linearity in the loading trace, termed the non-linear initiation point (NL); (b) by either the maximum load or the intersection of a line with the load trace which has a compliance 5% greater than the initial loading line (and taking whichever occurs first), termed the (Max/5%) initiation point; and (c) when the crack is seen to move by the operator viewing the side of the specimen with a microscope or video camera, termed the (VIS) initiation point. The length of the crack during crack propagation was determined during the test. For each value of crack length the corresponding values of load and displacement were measured.

3. Data Reduction Methods

3.1. Introduction

The initial protocol [10] and subsequent British Standard [12] specify that the adhesive fracture energy, G_{IC}, of the joints be determined at each value of the crack length using three analysis methods namely, simple beam theory (SBT), corrected beam theory (CBT) and an experimental compliance method (ECM). This approach is followed to allow comparison with the ASTM standard analysis procedures [7] and also to allow a cross check on the level of agreement between the beam theory and compliance methods of analysis. The work-area method was not employed because the required periodic unloading and reloading of the joint would be tedious to perform and it has been shown [8, 15] that the accuracy of the method was inferior to the CBT or ECM methods. In addition, the work-area method is unsuitable for analysing stick-slip crack growth, which is occasionally observed when testing adhesive joints. All data analysis in the round-robin was performed using *Microsoft Excel*© spreadsheets. These automatically performed all the data reduction and plotted the linear regression analyses and the R-curves. Spreadsheets compatible with the British Standard [12] are available to download free of charge from the Imperial College website: http://www.me.ic.ac.uk/materials/AACgroup.

The three analysis methods essentially all stem from the Irwin-Kies equation (1) in which the adhesive fracture energy, G_{IC}, is deduced directly from:

$$G_{IC} = \frac{P^2}{2B} \cdot \frac{dC}{da} \qquad (1)$$

where P is the applied load, B is the width of the joint, C is the compliance and a the crack length. The different forms of analysis each use different schemes to solve for dC/da. The analysis schemes employed will now be briefly outlined.

3.2. Simple Beam Theory (SBT)

The simple beam theory (SBT) method was based upon the shear corrected beam analysis derived by Mostovoy and co-workers [6] and implemented in the ASTM standard [7]. In this

work it was shown that, for thin adhesive layers, the compliance of the beam, *C*, could be expressed as:

$$C = \frac{8\left(a^3 + h^2 a\right)}{E_s B h^3} \tag{2}$$

where *h*, *B* and E_s are the height, width and Young's modulus of the substrate respectively. Differentiating equation (2) and substituting into equation (1) leads to:

$$G_{IC} = \frac{4P^2}{E_s B^2}\left(\frac{3a^2}{h^3} + \frac{1}{h}\right) \tag{3}$$

From this analysis, the shape of the tapered double cantilever beam was proposed [7], such that the value of the term in brackets in equation (3) was held constant and termed *m*, such that:

$$m = \frac{3a^2}{h^3} + \frac{1}{h} \tag{4}$$

In the present work, the value of *m* was always equal to 2mm^{-1} for the TDCB joints. This form of analysis is applicable to both the DCB and the TDCB geometry however, for the DCB the value of *m* is, of course, not constant.

3.3. Corrected Beam Theory (CBT)

The simple beam theory described above considers the deflections of the beam due to bending and shear but does not account for the important effects of beam root rotation. Root rotation affects both the compliance of the beam and the resulting values of G_{IC}. Williams [16] showed that the effects of both shear deflection and root rotation could be modelled for a DCB specimen by adding a length, Δ, to the measured crack length thus:

$$C = \frac{8\left(a + |\Delta|\right)^3}{E_s B h^3} \cdot N \tag{5}$$

The correction Δ may be found from the negative intercept of a plot of $C^{1/3}$ versus a. If the DCB is loaded via bonded on end-blocks, as is usually the case when CFRP substrates are employed, then a correction factor, N, is applied to equation (5) as shown, to correct for stiffening by the presence of the end-blocks and the rotation of the block. If the load is applied to the DCB specimen via holes drilled directly through the substrates then N=1 in equation (5). Differentiating equation (5), eliminating E_s and substituting into equation (1) leads to:

$$G_{IC} = \frac{3P\delta}{2B(a+|\Delta|)} \cdot \frac{F}{N} \tag{6}$$

where δ is the measured load-line displacement and F is a correction factor which accounts for the reduction in bending moment caused by large displacements. Again, if drill holes are used to apply the load, then N=1. The corrections F and N were derived in [17] and are given by:

$$F = 1 - \frac{3}{10}\left(\frac{\delta}{a}\right)^2 - \frac{3}{2}\left(\frac{l_1\delta}{a^2}\right) \tag{7}$$

$$N = 1 - \left(\frac{l_2}{a}\right)^3 - \frac{9}{8}\left[1 - \left(\frac{l_2}{a}\right)^2\right]\frac{l_1\delta}{a^2} - \frac{9}{35}\left(\frac{\delta}{a}\right)^2 \tag{8}$$

where l_1 and l_2 are load block dimensions defined in the protocol.

In the simple beam theory analysis for the tapered double cantilever beam specimen described above, two simplifications were made. Firstly, no correction for beam root rotation was applied and secondly the shape of the beam was assumed to be profiled over the entire length of the joint, i.e. tapering to zero height at zero crack length. Of course, to be able to test the joint, extra material is needed and this extra material alters the compliance. Considering the effects of both beam root rotation and the real, as opposed to idealised profile of the beam, the compliance of the TDCB specimen may be written as [11]:

$$C = \frac{8m}{EB}\left(a + 0.64\left(\frac{3}{m}\right)^{\frac{1}{3}} \cdot a^{\frac{2}{3}} - \frac{2}{3}x_o \right) \tag{9}$$

where x_o is the distance between the load line and the start of the taper. Differentiating equation (9) and substituting into equation (1) leads to:

$$G_{IC} = \frac{4P^2}{E_s B^2} \cdot m \cdot \left[1 + 0.43\left(\frac{3}{ma}\right)^{\frac{1}{3}} \right] \tag{10}$$

In the round-robin, m was always equal to 2mm^{-1} for the TDCB specimens. The round-robin provided the motivation to develop equations (9) and (10) because all the data was analysed using the spreadsheets and consistent errors between the values of G_{IC} deduced via the SBT and ECM approaches were always evident in the results, as was discussed in [11] and will be further highlighted in the results section of the present work.

3.4. Experimental Compliance Method (ECM)

In the experimental compliance method, equation (1) is used directly to determine G_{IC}. For the analysis of the DCB test, Berry's method [18] has been implemented in the protocol. This employs a power-law compliance calibration of the form:

$$C = ka^n \tag{11}$$

where k and n are experimentally determined constants. Differentiating equation (11) and substituting into equation (1) leads to:

$$G_{IC} = \frac{nP\delta}{2Ba} \cdot \frac{F}{N} \tag{12}$$

where F and N are applied if appropriate. The constant n may be determined by the slope of a plot of log C versus log a as described in the standard [12]. For the tapered double cantilever beam test specimen, a plot of C versus a is linear and hence the value of dC/da is constant.

Hence, for this test specimen, dC/da is determined directly from a linear regression analysis of the C versus a data, and equation (1) is then employed to deduce G_{IC}.

3.5. Back-calculated modulus

The corrected beam theory may be used to back-calculate the modulus of the substrate, termed E_f (note that the subscript used differentiates between the value back-calculated from flexural stiffness '*f*' and the known or independently measured value for the substrate '*s*'). This is a very useful cross-check on the accuracy of the experimental results as a value independent of crack length should be obtained. In the protocol, it is recommended that the variation in E_f is deduced for each test, and if this variation is more than 10% of the average value for the test, then the values of G_{IC} should be considered suspect. Also, the value of E_f may be compared to the independently measured or accepted value for the substrate, E_s to check accuracy. It is common for the value of E_f to exceed the known value, E_s but a large discrepancy would imply suspect results. The value of E_f is deduced by rearranging equation (5), thus:

$$E_f = \frac{8\left(a + |\Delta|\right)^3}{\frac{C}{N} Bh^3} \tag{13}$$

If drill holes or piano hinges are used to introduce the load, then N=1.

Similarly, the corrected beam theory may be employed to calculate a value of dC/da for the TDCB specimen [11]. The value of dC/da may be expressed as:

$$\frac{dC}{da} = \frac{8m}{EB}\left(1 + 0.43\left(\frac{3}{ma}\right)^{\frac{1}{3}}\right) \tag{14}$$

This value can be compared to the experimental value, a useful cross-check on the analysis, as if the value of dC/da differs significantly from the experimental value the results should be considered suspect.

4. Results and Discussion

4.1. Introduction

The participating laboratories were asked to enter all the required data into the analysis spreadsheets after the tests. The spreadsheets automatically calculated the values of G_{IC} according to the protocol [10]. These data files were then returned to the present authors for further analysis. All the results from the round-robin have been analysed according to statistical guidelines outlined in the International Standard for the analysis of inter-laboratory data [19], as described later.

4.2. Load-displacement behaviour

Typical load-displacement traces for the joints tested in the round-robin are shown in Figures 2 and 3. Figure 2 shows the re-loading from the mode I precrack, testing and final unloading for a mild steel DCB joint. Some initial non-linearity in the loading trace is commonly encountered in fracture testing due to load take up effects and the fact that cross-head displacement is recorded rather than the actual beam opening displacement. The protocol describes how these effects should be treated. Essentially, the initial non-linearity in the loading curve is removed by extrapolating the linear part of the trace back to zero load and by resetting the intercept to zero displacement. This line is shown in Figure 2 with the originally measured displacement values. The unloading curve may also show some final non-linearity at low loads, and thus the true final unloaded point may be found by the extrapolation of the linear part of this curve back to zero load. This is shown as the third fitted line in Figure 2. The second fitted line represents the 5% increase in initial compliance line that is drawn to determine the 5% change in compliance value of initiation. The horizontal distance between the first and the third fitted lines at zero load is termed the offset displacement, δ_{offset}, and this value was recorded by participating laboratories for each test. For the test shown in Figure 2, which was a typical result, the value of δ_{offset} was 0.06mm, thus the ratio of $\delta_{offset}/\delta_{max}$ was 0.039 for this joint, i.e. within the 0.05 limit suggested in the protocol and implying that no permanent deformation of the substrates had occurred. This conclusion was supported by visual inspection of the beams after the test.

Figure 3 shows a typical loading trace obtained during a TDCB test for a joint manufactured with aluminium alloy substrates. Three fitted lines have been drawn as before. Prior to analysis, the displacement axis would have been again re-zeroed at the point of intersection

with the first fitted line. For the joint of Figure 3, the ratio of $\delta_{offset}/\delta_{max}$ was 0.042 and visual inspection of the substrates after testing again confirmed that no plastic deformation of the beams had resulted. For this adhesive joint, there was a very gradually rising plateau load following initiation. This led to a modestly rising R-curve for this joint, as will be discussed later. For the mild steel TDCB joints the load remained constant following crack initiation and thus rising R-curves were not observed for this joint system.

4.3. The effects of system compliance

Following the round-robin, participants were asked to measure the compliance of the tensile loading system that they had used, as it had become apparent that significant displacement errors could be introduced when the very stiff steel DCB specimens were tested. This had resulted in very high values of the back-calculated modulus, E_f, being determined and a correspondingly high beam theory correction term, $|\Delta|$ being deduced. The protocol warns that if the value of E_f differs significantly from the known value E_s, then the results are considered suspect.

The protocol was modified *a posteriori* to incorporate a system compliance correction and this is now embodied in the British Standard [12]. A very rigid coupling is used to link the two loading shackles, with the test system set up in exactly the same manner as the fracture tests. Figures 4(a) and (b) depict repeated load-displacement traces for the system compliance correction performed by one of the participating laboratories. Figure 4(a) shows the load-displacement traces for six repeat loadings and Figure 4(b) shows these data corrected for the initial non-linear take-up-of-play effects, which are also removed from the fracture loading curves as previously described. This laboratory measured a mean system compliance value of 1.008×10^{-4} mm/N, corresponding to a system stiffness of 9.92kN/mm. The values of system compliance measured in the different laboratories for the very different test machines and shackle arrangements employed ranged widely, from 1.8×10^{-4} to 2.0×10^{-5} mm/N, corresponding to stiffness values of 5.55 to 50.0kN/mm. This wide range of machine stiffness values obtained by the participating laboratories emphasises the need to make this compliance correction if accurate and reproducible results are to be deduced.

The system compliance was used to correct the measured displacement, δ, leading to a lower specimen compliance than was initially measured. The effect of this correction on the DCB data reduction can be observed in Figure 5. This shows a graph of $(C/N)^{1/3}$ versus crack

length for a DCB manufactured with mild steel substrates. Both corrected and uncorrected data are shown. The machine stiffness in this case was 8.92kN/mm. Prior to applying the system compliance correction, the plot of $(C/N)^{1/3}$ versus crack length intercepted the a axis at –55.9mm, implying a beam theory correction term $|\Delta|$ =55.9mm and the back calculated modulus, E_f, obtained from equation (13) was equal to 354GPa. Now, as the substrates were mild steel, a modulus E_s of 207GPa should have been obtained, implying an error in E_f of 71%, clearly a suspect result. Following the correction for system compliance, Figure 5 indicates a $|\Delta|$ of 17.9mm and an E_f of 210GPa. Thus, for these rather stiff DCB specimens, the system compliance correction had a very significant effect on both the values of $|\Delta|$ and E_f.

The effect of the system compliance correction on the TDCB data reduction can be observed in Figure 6. This shows a graph of compliance versus crack length for a TDCB joint made using aluminium alloy substrates. These data were corrected using a system stiffness value of 8.92kN/mm. The effect of the correction is to lower all the compliance values, but without changing the slope of the C vs a line. Because the adhesive fracture energy, G_{IC} is proportional to this slope, the correction has little effect on the values of G_{IC} calculated. However, the implied intercept of this line with the a-axis was altered and changes from +7.4mm for the uncorrected data to +20.3mm for the corrected data. The significance of this intercept value was discussed in [11], but it is sufficient to note here that the corrected beam theory of equation (9) predicts an intercept of +26mm for these beams, and so the system compliance correction has yielded better agreement between the experimental compliance and the compliance deduced via the CBT method.

Whilst the correction had little effect on values of G_{IC} calculated for the TDCB joints, a more pronounced effect was noted for the mild steel DCB joints. Figure 7(a) shows the R-curves for the mild steel joint of Figure 5 (uncorrected data) deduced via the three analysis methods, namely SBT, CBT and ECM. A striking feature of this graph is the apparent decrease in the values of G_{IC} with crack length when deduced via either the CBT or ECM analysis methods. This is not a reasonable result, as G_{IC} should not decrease with increasing crack length during stable growth. However, Figure 7(b) shows the data corrected for the effects of system compliance and it can be seen that the values of G_{IC} determined via the CBT and ECM methods now show no decrease, with a flat R-curve now being obtained. The SBT approach is unaffected by this correction (as the correction is implemented via displacement). Also,

Figure 7(b) clearly shows that the SBT analysis method is in disagreement with the ECM and CBT analysis methods, and is indeed incorrect as will be discussed later.

4.4. Crack initiation values of G_{IC}

The protocol requires that values of crack initiation be determined from both the insert film and from the mode I precrack generated during initial testing. This requirement is consistent with the mode I composites standard [9] and is designed to ensure that the values are not influenced by the presence of the insert film. As such, conservative initiation values can be reliably determined. Non-linear (NL), visual (VIS) and the maximum load or 5% change in compliance values (Max/5%) are measured.

Thus, for each of the four adhesive joints investigated, the six values of initiation were deduced for each laboratory, i.e. three values from the insert and three from the mode I pre-crack. The spreadsheets automatically deduced the initiation values of G_{IC} via the three analysis schemes for the participants, but for clarity only the results obtained using the CBT analysis method are presented here. The results followed the same basic pattern for each joint type, so just one will be described. Figure 8(a) shows the results obtained from the insert for the mild steel TDCB substrates that were tested by laboratories 1-5. Figure 8(b) shows the results measured from the mode I precrack. Laboratory 1 did not report any initiation values and so no data appears for this laboratory. Figure 8(c) combines the data of Figures 8(a) and 8(b) to aid the comparison.

From these data several observations can be made. Firstly, it can be seen that, in general, values of initiation from the insert film were somewhat lower than the equivalent values from the mode I precrack. This indicates that the 12.5μm thick PTFE insert film used in this study worked well and generated a sharp initial crack which yielded lower initiation G_{IC} values than were obtained from the mode I precrack. Secondly, it can be seen that for initiation from either the insert film or mode I precrack, then the most conservative initiation values of G_{IC} were obtained from the non-linear definition point, i.e. NL point. Thirdly, the least conservative initiation G_{IC} values were usually deduced from the Max/5% definition, thus the trend in G_{IC} (initiation) values was Max/5%>VIS>NL. The precision of these data will be discussed later.

The results obtained do raise the question of whether the precracking stage is necessary. The precracking requirement was written into the protocol to ensure that conservative values of G_{IC} at initiation were always measured. Certainly from these results the insert film has worked well and has generated conservative values. However, this might not always be the case, and when different insert films and/or more brittle adhesives are used, then precracking may be important. If the precracking is omitted, then this check cannot be made.

4.5. Mean crack propagation values of G_{IC}

The protocol requires that the R-curves be constructed for each test to show how the values of G_{IC} develop during crack growth. Figure 7(b) showed typical R-curves for the mild steel DCB joint. To enable the data to be statistically compared across the different laboratories, a mean propagation value of G_{IC} was determined for each test. This was simply the mean of all the non-initiation G_{IC} values. A mean propagation value of G_{IC} was determined for each test using the three forms of analysis i.e. SBT, CBT and the ECM methods. Figures 9-12 show these mean propagation values of G_{IC} for the different joints tested in the round-robin. Figure 9 shows the results for the DCB joints manufactured with CFRP substrates as tested by laboratories 1-5. The height of the columns represents the mean values, and the error bars the standard deviations within each laboratory. Figure 10 shows the results for the DCB joints manufactured with the mild steel substrates as tested by laboratories 6-10. Figures 11-12 show the propagation values of G_{IC} for the testing of the TDCB specimens: Figure 11 shows the mild steel substrates and Figure 12 the aluminium alloy substrates.

The propagation results are noteworthy for several reasons. Firstly, all propagation values of G_{IC} deduced via the SBT analysis are lower than the equivalent values deduced via either the CBT or ECM analysis methods, which agree closely. This is consistent with the conclusion that the SBT analysis method is inaccurate due to the incorrect assumptions made in its derivation. The error in the values of G_{IC} deduced via the SBT analysis are greatest for the DCB joints manufactured with mild steel substrates. For these joints, SBT yields values of G_{IC} about 30% below either of the other analysis methods. Clearly for these joints, neglecting the crack root rotation (as in the SBT analysis method) leads to very substantial errors.

Secondly, the values of G_{IC} appear to be strongly dependent upon which substrate was used to make the joint. This was a surprising finding, as all failures were reported to be cohesive-in-the-adhesive layer, and thus no interfacial failure was seen. Also, the adhesive layer thickness

had been kept constant in all joints, so the variations in G_{IC} could not be ascribed to differences in bondline thickness. This observation has led the present authors to undertake a further study into the dependence of G_{IC} values on substrate material used, the initial results of which can be found in [20]. In this study, the value of G_{IC} measured in the fracture tests were shown to correlate closely with the values of the glass transition temperature, T_g, of the cured adhesive. The T_g values were measured by performing differential scanning calorimetry on samples of adhesive removed from the fracture surfaces after testing. The lower values of T_g for the adhesive removed from CFRP joints was shown to be the result of pre-bond moisture present in the composite substrates. Removing all pre-bond moisture from the CFRP substrates prior to bonding resulted in higher values of G_{IC} being measured (equivalent to that obtained when mild steel substrates were employed) and also similar values of T_g to those obtained from the steel substrates were measured [20]. Also, by carefully controlling the heat-up rate, similar values of T_g for the adhesive layer in the aluminium alloy and mild steel joints could be achieved, and this then led to very similar values of G_{IC} being measured. Indeed, the correlation between T_g and G_{IC} is shown in Figure 13 for the joints tested in the round-robin and for additional joints prepared with different values of T_g for the cured adhesive. As noted above, the values of T_g were varied by either controlling the level of pre-bond moisture in the CFRP substrates, or by changing the heat-up rate during cure for the aluminium alloy joints.

Thirdly, the results for the DCB and TDCB specimens manufactured from mild steel (see Table 3 and Figures 10 and 11) were equivalent, indicating that there was no geometry dependence upon the G_{IC} value measured by the two test specimens. Finally, the back-calculated values of flexural modulus, E_f, for the DCB specimens made with CFRP substrates were all independent of crack length and were in the range 144-171GPa for the five laboratories, showing close agreement with the independently measured value of 150GPa. For the DCB specimens made with mild steel substrates, all but one laboratory reported values for E_f in the range 213-249GPa, again showing close agreement with the accepted value of 207GPa. The values were again all independent of crack length. The statistical procedures used for analysing the round-robin data are now discussed.

4.6. Precision analysis

The accuracy (trueness and precision) of the measurement methods and results have been deduced according to the International Standard [19]. Firstly, the different levels of the

property, G_{IC}, were identified as follows. The test method produces six different values of initiation fracture energy (i.e. three from the insert and three from the precrack) and typically fifteen propagation values for a stable test. These values are then repeated for each of the three different analysis schemes employed, yielding a very large results table. To simplify the precision analysis, the initiation values of G_{IC} have been deduced using the CBT analysis method only. Also, as the joints tested showed no strongly rising R-curve behaviour, only the mean propagation values of G_{IC} have been considered in the statistical analysis. Thus, for crack initiation, six values of G_{IC} are reported for each test, representing six levels of the property in the statistical analysis. For crack propagation, a mean propagation value of G_{IC} has been determined using the three analysis schemes for each test, representing three levels of the property in the statistical analysis. Thus, the statistical analysis has nine levels for each of the four adhesive test specimens employed, i.e. 36 levels in total.

The basic scheme used in the statistical analysis was as follows. Firstly, all the original data for each laboratory at each level was compiled into a table with each test specimen type being considered separately. Any obviously discordant data was investigated and discussed with the participants to try to find out the source of the problem. For example, one laboratory reported that an error in displacement measurement had occurred during all their TDCB tests. This could not be rectified afterwards and so the values of G_{IC} requiring the displacement value, i.e. the ECM method, were discarded for that laboratory. However, very little data had to be excluded during the course of the statistical analysis, indicating the general soundness of the test method. The means and standard deviations were then calculated for each cell, i.e. for each laboratory at each level. The grand mean was then calculated for each level, i.e. for all laboratories. At this stage, various statistical tests were applied to the results.

The precision values for the test methods were then deduced, i.e. the mean, the repeatability standard deviation S_r and the reproducibility standard deviation S_R were determined. The repeatability standard deviation, S_r, is a measure of the average within laboratory variation and the reproducibility standard deviation, S_R, is a measure of the average inter-laboratory variation. These precision values are shown in Tables 2 and 3 for initiation and propagation values for G_{IC} respectively. The tables show the precision values for each joint system individually with the values of S_r and S_R also expressed as a percentage of the mean (percentage values in brackets). Due to the lower mean values of G_{IC} measured for the DCB joints made with CFRP substrates, and the variation in the values of G_{IC} resulting from the

pre-bond moisture levels in the substrates not being controlled, the values of S_r and S_R expressed as a percentage of the mean are correspondingly higher for these joints. For initiation it can be seen from Table 2 that in general the lowest values of S_r and S_R were obtained from the Max/5% definition, indicating that this definition yielded the most repeatable and reproducible results. The repeatability and reproducibility of the visual initiation values of G_{IC} for the mild steel DCB joints was relatively poor, reflecting the difficulty in detecting crack initiation when the displacements were very small, i.e. when using very stiff substrate arms. The values of S_r and S_R for the NL and VIS definitions were broadly similar for the TDCB joints. The mild steel TDCB specimen yielded the lowest values of S_r and S_R for crack initiation.

In terms of crack propagation, Table 3 reveals that the CBT and ECM analysis methods yield very similar precision values, with both the repeatability and reproducibility standard deviations being about 6%. The mild steel TDCB precision data indicate that the variability in the SBT analysis method was equivalent to the CBT analysis method at about 8% as expected. However, the larger values of S_r and S_R of 13% and 17% respectively for the ECM analysis method indicate its poorer performance in this case. Finally, the aluminium alloy TDCB precision results indicate that generally larger percentage values of S_r and S_R were deduced than for joints manufactured with mild steel substrates. This was partly due to the lower mean values of G_{IC} deduced for the aluminium alloy TDCB specimens and also partly due to the consistently low results reported by Laboratory 9 and the high standard deviations reported by Laboratory 8. However, these data were not identified as outlying by the statistical tests and were thus retained.

It is obviously of interest to compare the precision values obtained here with the values from other standardized fracture mechanics test methods. For example, the ISO standard for measuring the plane strain fracture toughness for bulk polymers [21] reported average standard deviations (S_r values) of 12% in the values of G_{IC} obtained. Also, the mode I test standard for composite delamination [9] quoted values of S_r typically of about 10% and values of S_R in the range of 8% to 19%. Although it should be noted that values of standard deviation are likely to be higher for a brittle material than a tough one, the precision values obtained for this mode I structural adhesive joint test do compare favourably with these reported values, indicating the soundness of the method.

Conclusions

The results from the inter-laboratory round-robin highlighted the importance of correcting for system compliance effects if accurate and reproducible results are to be obtained. Such system compliance effects were shown to lead to large errors in the back-calculated modulus values and large beam theory corrections being required. When the compliance correction was made, the back-calculated values of flexural modulus were independent of crack length and close to the independently measured value, validating the corrected beam theory (CBT) analysis employed. The most conservative values of G_{IC} were determined directly from the insert film, with the non-linear definition of initiation yielding the lowest values and the Max/5% definition yielding the best repeatability. Simple corrected beam theory (SBT) was shown to be in error, and more accurate values of G_{IC} were obtained from either the corrected beam theory (CBT) or experimental compliance method (ECM) approaches. The values of G_{IC} deduced were shown to be independent of test geometry (i.e. DCB versus TDCB) but dependent upon the substrate material used to make the joints. Additional studies have shown that the substrate dependence was due to the cured adhesive in the different joints possessing different values of glass transition temperature. The existence of pre-bond moisture in the CFRP substrates and variations in heat-up rate during cure were both shown to affect the T_g of the cured epoxy-paste adhesive employed in the present work. The pre-bond moisture effect was however, much more important than the heat-up rate effect but both would need to be considered when optimising joints for toughness with the present adhesive.

Acknowledgements

The authors wish to thank the technical committee TC4, of the European Structural Integrity Society (ESIS) under the joint chairmanship of Professors J.G. Williams and A. Pavan for providing the framework within which this International round-robin operated. In particular, we wish to thank the following participants and their employing organisations (many of which contributed financially to the costs of specimen manufacture): Professor Belzunce (Universidad de Oviedo, Spain), Dr M. Paraschi (Imperial College, UK), Dr P. Davies (IFREMER, France), Dr G. Orange (Rhodia Recherches, France), Dr F. Ramsteiner (BASF, Germany), Dr Fontanari (University di Pisa, Italy), Dr D. Hunston (NIST, USA), Dr J. Harris (MERL, UK), Professor A. Pavan (Politecnico di Milano, Italy) and Drs P. Habets & S. Holton (DSM, Netherlands). For general financial support, the authors wish to thank the EPSRC (Advanced Fellowship AF/992781) and the National Physical Laboratory. We also

wish to thank Mr T. Robinson for specimen manufacture and Permabond (UK) and Cytec Fiberite for material supply.

References

1. Kinloch, A.J., *Adhesion & Adhesives: Science & Technology*. 1987, London & New York: Chapman Hall.
2. Blackman, B.R.K., A.J. Kinloch, A.C. Taylor, and Y. Wang, *The impact wedge-peel performance of structural adhesives.* Journal of Materials Science, 2000. **35**: p. 1867-1884.
3. Yang, Q.D., M.D. Thouless, and S.M. Ward, *Analysis of the symmetrical 90 degree peel test with extensive plastic deformation.* Journal of Adhesion, 2000. **72**: p. 115-132.
4. Georgiou, I., H. Hadavinia, A.J. Kinloch, V. Tropsa and J.G. Williams, *Cohesive zone models and the plastically deforming peel test.*, Accepted for publication in Journal of Adhesion 2003.
5. Ripling, E.J., S. Mostovoy, and R.L. Patrick, *Measuring fracture toughness of adhesive joints.* Materials Research & Standards (ASTM Bulletin), 1964. **4**(3, March): p. 129-134.
6. Mostovoy, S., P.B. Crosley, and E.J. Ripling, *Use of crack-line loaded specimens for measuring plane-strain fracture toughness.* Journal of Materials, 1967. **2**(3): p. 661-681.
7. *ASTM D3433*, in *Annual book of ASTM standards. Adhesives section 15*. 1990: Philadelphia.
8. Hashemi, S., A.J. Kinloch, and J.G. Williams, *The analysis of interlaminar fracture in uniaxial fibre-polymer composites.* Proceeding of the Royal Society London, 1990. **A427**: p. 173-199.
9. ISO, *Standard test method for the mode I interlaminar fracture toughness, G_{IC}, of unidirectional fibre-reinforced polymer matrix composites.* **ISO 15024: 2001**.
10. Blackman, B.R.K. and A.J. Kinloch, *Determination of the mode I adhesive fracture energy, G_{IC}, of structural adhesives using the double cantilever beam (DCB) and the tapered double cantilever beam (TDCB) specimens. Version 97-04.* ESIS TC4 Protocol,(1997).

11. Blackman, B.R.K., H. Hadavinia, A.J. Kinloch, M. Paraschi and J.G. Williams, *The calculation of adhesive fracture energies in mode I: Revisiting the tapered double cantilever beam (TDCB) test.* Engineering Fracture Mechanics, 2003. **20**: p. 233-248.
12. BSI, *Determination of the mode I adhesive fracture energy, G_{IC}, of structural adhesives using the double cantilever beam (DCB) and tapered double cantilever beam (TDCB) specimens.* 2001. **BS 7991**.
13. Atkins, A.G. and Y.W. Mai, *Elastic and plastic fracture.* Ellis Horwood Series: Engineering Science. 1985, Chichester:Ellis Horwood. p. 169.
14. Kinloch, A.J. and R.J. Young, *Fracture behaviour of polymers.* 1983, London: Chapman and Hall. p295.
15. Blackman, B.R.K., Dear, J.P., Kinloch, A.J. and Osiyemi, S. *The calculation of adhesive fracture energies from double-cantilever beam test specimens.* Journal of Materials Science Letters, 1991. **10**: p. 253-256.
16. Williams, J.G., *End corrections for orthotropic DCB specimens.* Composites Science and Technology, 1989. **35**: p. 367-376.
17. Williams, J.G., *Large displacement and end block effects in the DCB interlaminar test in modes I & II.* Journal of Composite Materials, 1987. **21**(April): p. 330-347.
18. Berry, J.P., *Some kinetic considerations of the Griffith criterion of fracture-I; Eqns of motion at constant deformation.* J. Mech. Phys. Solids, 1960. **8**: p. 207-216.
19. ISO, *Accuracy (trueness and precision) of measurement methods and results. Part 2. Basic methods for the determination of repeatability and reproducibility of a standard measurement method.* 1994. **ISO 5725-2**.
20. Blackman, B.R.K., A.J. Kinloch, and M. Paraschi, *The effect of the substrate material on the value of the adhesive fracture energy, Gc: Further considerations.* Journal of Materials Science Letters, 2001. **20**: p. 265-267.
21. ISO, Plastics-*Standard test method for the determination of fracture toughness (G_c and K_c)- A linear elastic fracture mechanics approach.* ISO Standard, 2000. **ISO 13586**.

LIST OF TABLES

Table 1.

Details of the adhesive joint systems manufactured

Description	DCB/CFRP	DCB/Mild-steel	TDCB/Mild-steel	TDCB/Al-alloy
Joint type	DCB	DCB	TDCB	TDCB
Substrate	CFRP	Mild-steel	Mild-steel	Al-alloy
B (mm)	20	25	10	9.85
h (mm)	1.65	20	*	*
h_a (mm)	0.4	0.4	0.4	0.4
E_s (GPa)	150	207	207	71

(Notes: B= width of joint, h= thickness of one substrate arm, h_a=thickness of adhesive layer and E_s=substrate axial modulus. * implies tapered with m=2mm^{-1})

Table 2.

Precision data for the initiation values of G_{IC} calculated using the CBT analysis method.

		G_{IC} (Insert) (J/m^2)			G_{IC} (Precrack) (J/m^2)		
Joint		NL	VIS	Max/5	NL	VIS	Max/5
	mean	140	151	202	165	186	225
CFRP	S_r (%)	52 (37%)	40 (27%)	78 (39%)	83 (50%)	69 (37%)	106(47%)
DCB	S_R (%)	58 (41%)	43 (28%)	73 (36%)	93 (57%)	92 (49%)	92 (41%)
	mean	551	636	753	706	745	857
Mild steel	S_r (%)	84 (15%)	82 (13%)	79 (10%)	61 (9%)	130(17%)	88 (10%)
DCB	S_R (%)	100(18%)	146(23%)	100(13%)	56(8%)	181(24%)	88(10%)
	mean	719	866	870	805	865	971
Mild steel	S_r (%)	71 (10%)	104(12%)	76(9%)	98(12%)	90(10%)	49(5%)
TDCB	S_R (%)	85(12%)	98(11%)	72 (8%)	106(13%)	107(12%)	54(6%)
	mean	453	560	606	535	532	622
Al-alloy	S_r (%)	73(16%)	113(20%)	67(11%)	78(15%)	114(21%)	107(17%)
TDCB	S_R (%)	83(18%)	117(21%)	117(19%)	135(25%)	165(31%)	170(27%)

Table 3.

Precision data for the mean propagation values of G_{IC}.

Joint		G_{IC}–mean propagation (J/m^2)		
		SBT	CBT	ECM
	mean	182	208	208
CFRP	S_r (%)	56 (31%)	70 (34%)	71 (34%)
DCB	S_R (%)	54 (30%)	65 (31%)	66 (32%)
	mean	636	918	920
Mild steel	S_r (%)	51 (8%)	50 (6%)	49 (5%)
DCB	S_R (%)	66 (10%)	58 (6%)	61 (6%)
	mean	873	958	960
Mild steel	S_r (%)	67 (8%)	74 (8%)	125 (13%)
TDCB	S_R (%)	74 (8%)	81 (8%)	158 (17%)
	mean	638	699	683
Al-alloy	S_r (%)	90 (14%)	99 (14%)	96 (14%)
TDCB	S_R (%)	98 (15%)	107 (15%)	100 (15%)

LIST OF FIGURES

Figure 7(b) A typical set of resistance curves for a DCB joint manufactured with the mild steel substrates and deduced via the three different analysis techniques (SBT, CBT and ECM methods). These data have been corrected for the effects of system compliance.

Figure 8(a). Initiation values of G_{IC} measured from the insert for the TDCB joints manufactured with the mild steel substrates as tested by laboratories 1-5. Values of the non-linear (NL), visual (VIS) and (Max/5%) definitions are shown. The height of the columns represent the within laboratory mean values and the error bars represent the within laboratory standard deviations. (Notes: Laboratory 1 did not report any initiation values and Laboratory 3 did not report any visual initiation values).

Figure 8(b). Initiation values of G_{IC} measured from the mode I precrack for the TDCB joints manufactured with the mild steel substrates as tested by laboratories 1-5. Values of the non-linear (NL), visual (VIS) and (Max/5%) definitions are shown. The height of the columns represent the within laboratory mean values and the error bars represent the within laboratory standard deviations. (Notes: Laboratory 1 did not report any initiation values and Laboratory 3 did not report any visual initiation values).

Figure 8(c). Comparison of initiation values of G_{IC} measured from the insert and from the mode I precrack for the TDCB joints manufactured with the mild steel substrates as tested by laboratories 1-5. Values of the non-linear (NL), visual (VIS) and (Max/5%) definitions are shown. The height of columns represent the within laboratory mean values and the error bars represent the repeatability standard deviation *S*r (see precision values).

Figure 9. The mean propagation values of G_{IC} for the DCB joints manufactured with the CFRP substrates as tested by laboratories 1-5. The values obtained using the different data reduction methods i.e. SBT, CBT and ECM methods are compared. The height of the columns represent the within laboratory mean values and the error bars represent the within laboratory standard deviations.

Figure 10. The mean propagation values of G_{IC} for the DCB joints manufactured with the mild steel substrates as tested by laboratories 1-5. The values obtained using the different data reduction methods i.e. SBT, CBT and ECM methods are compared. The height of the

columns represent the within laboratory mean values and the error bars represent the within laboratory standard deviations.

Figure 11. The mean propagation values of G_{IC} for the TDCB joints manufactured with the mild steel substrates as tested by laboratories 1-5. The values obtained using the different data reduction methods i.e. SBT, CBT and ECM methods are compared. The height of the columns represent the within laboratory mean values and the error bars represent the within laboratory standard deviations. (Note: Laboratory 3 ECM data was identified as outlying and was discarded).

Figure 12. The mean propagation values of G_{IC} for the TDCB joints manufactured with the aluminium alloy substrates as tested by laboratories 6-10. The values obtained using the different data reduction methods i.e. SBT, CBT and ECM methods are compared. The height of the columns represent the within laboratory mean values and the error bars represent the within laboratory standard deviations.

Figure 13. The correlation between the adhesive fracture energy, G_{IC}, and the glass transition temperature, T_g , of the cured adhesive in the joint. The joints tested in the round-robin are highlighted. The other data were measured in a separate study [20].

(a)

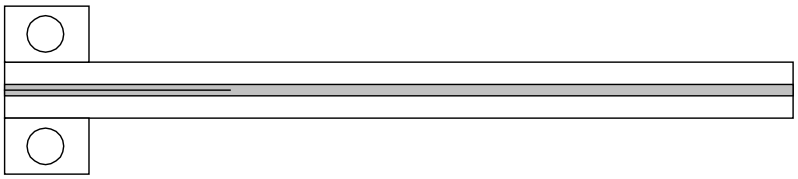

(b)

(c)

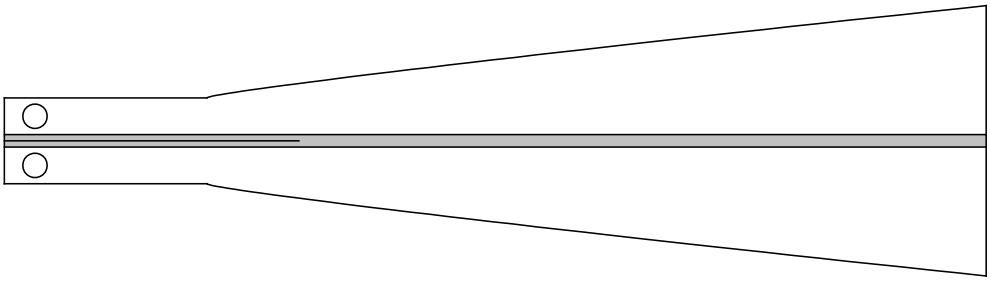

Figure 1. The adhesively bonded joints employed in the study: (a) the double cantilever beam (DCB) test specimen with load-blocks and (b) the double cantilever beam (DCB) test specimen with drill holes and (c) the tapered double cantilever beam (TDCB). Load is applied to the joints via pins inserted through the drill holes shown.

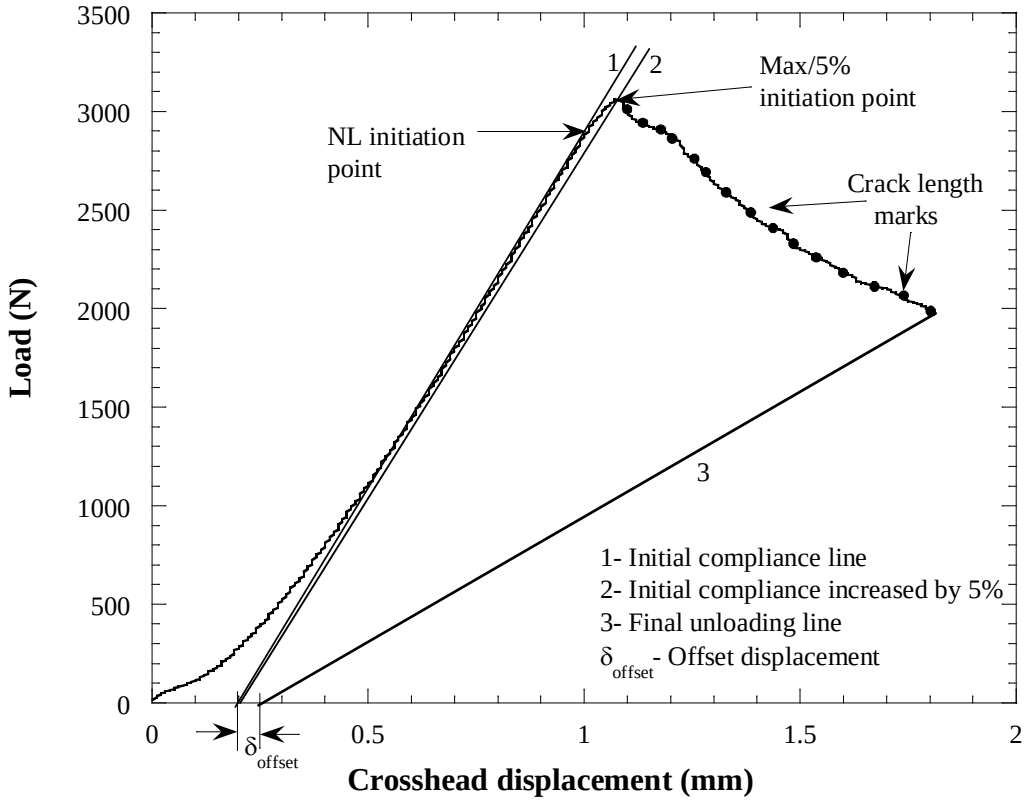

Figure 2. A typical load-displacement trace for a DCB joint manufactured with mild steel substrates, showing the loading and unloading lines drawn through the test data and also the $C_{5\%}$ line drawn for the determination of the Max/5% definition of initiation. The offset displacement, δ_{offset} is also shown between the initial compliance and unloading lines at zero load.

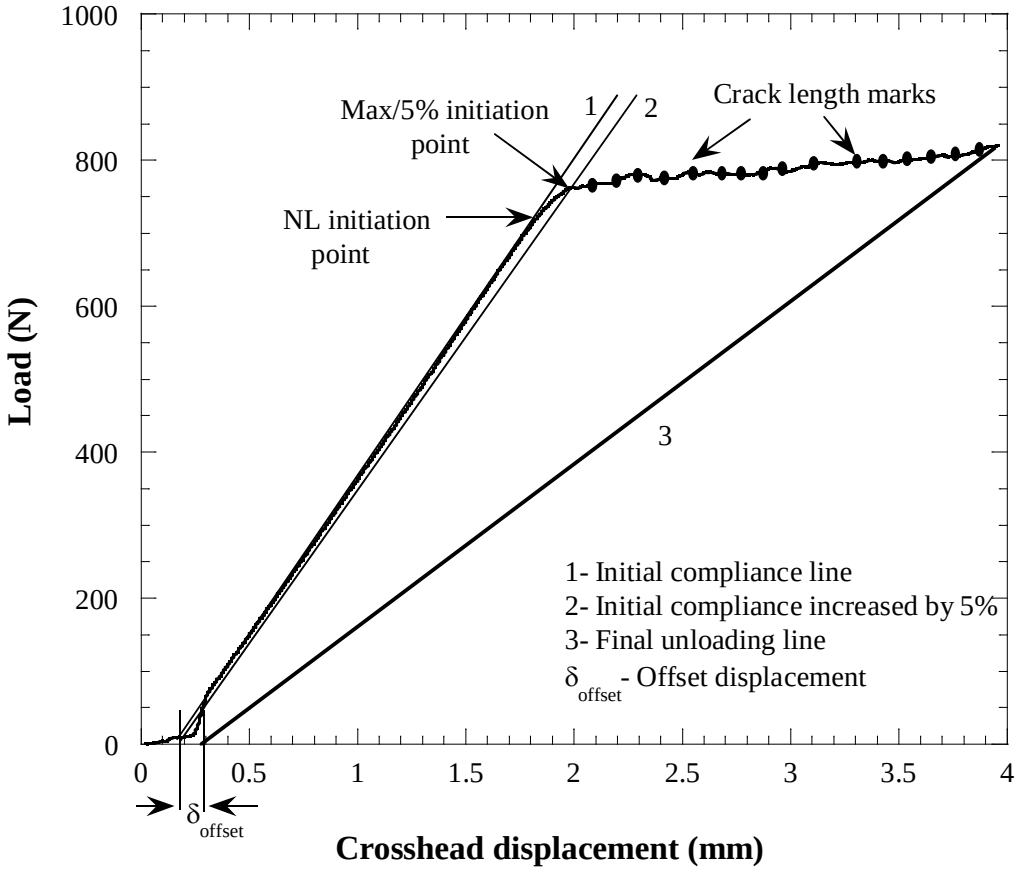

Figure 3. A typical load-displacement trace for a TDCB joint manufactured with aluminium alloy substrates, showing the loading and unloading lines drawn through the test data and also the $C_{5\%}$ line drawn for the determination of the Max/5% definition of initiation. The offset displacement, δ_{offset} is also shown between the initial compliance and unloading lines at zero load.

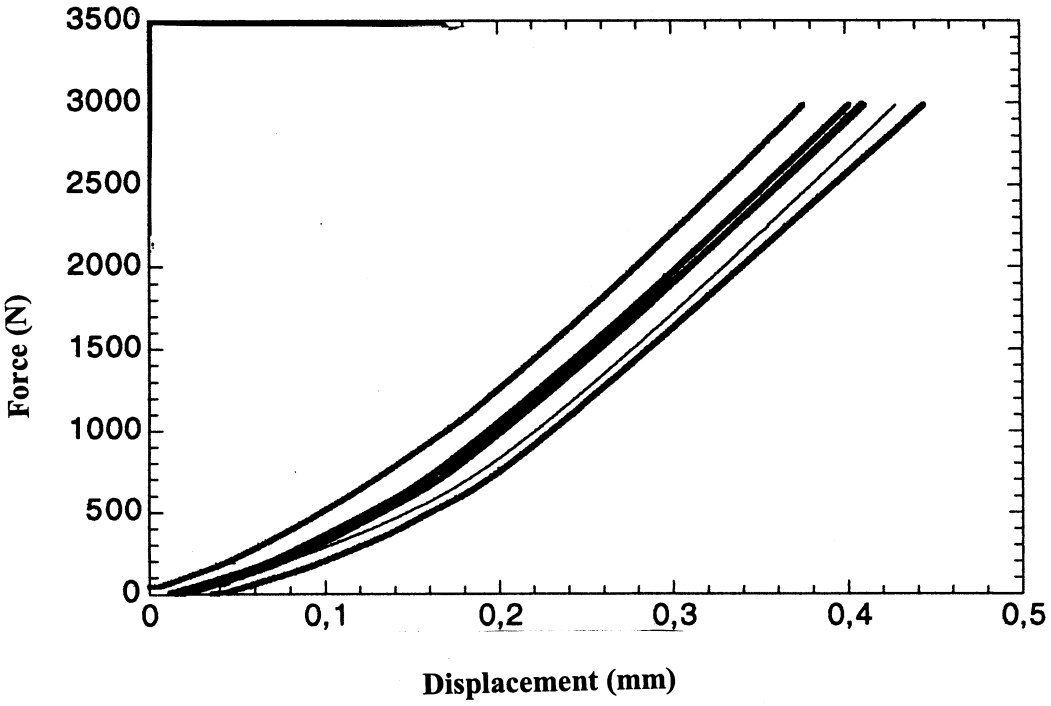

Figure 4(a) Several repeat force versus displacement traces measured during the system compliance calibration in one laboratory.

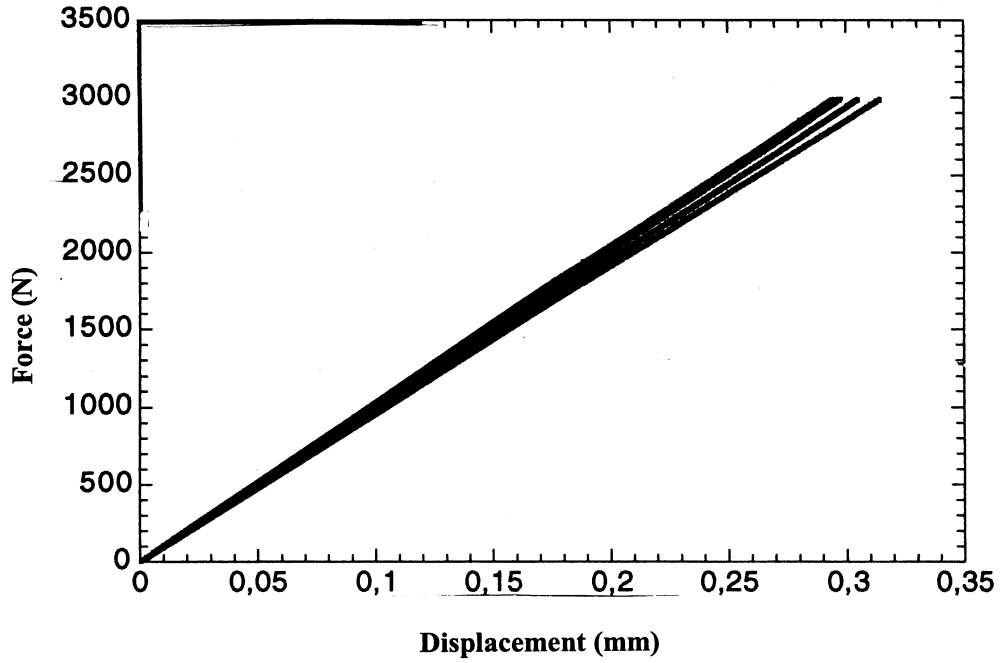

Figure 4(b) The traces in Figure 4(a) corrected for the initial non-linear effects due to take-up-of-play in the loading system. The system compliance measured in this laboratory was 1.008×10^{-4} mm/N (a system stiffness of 9.92 kN/mm).

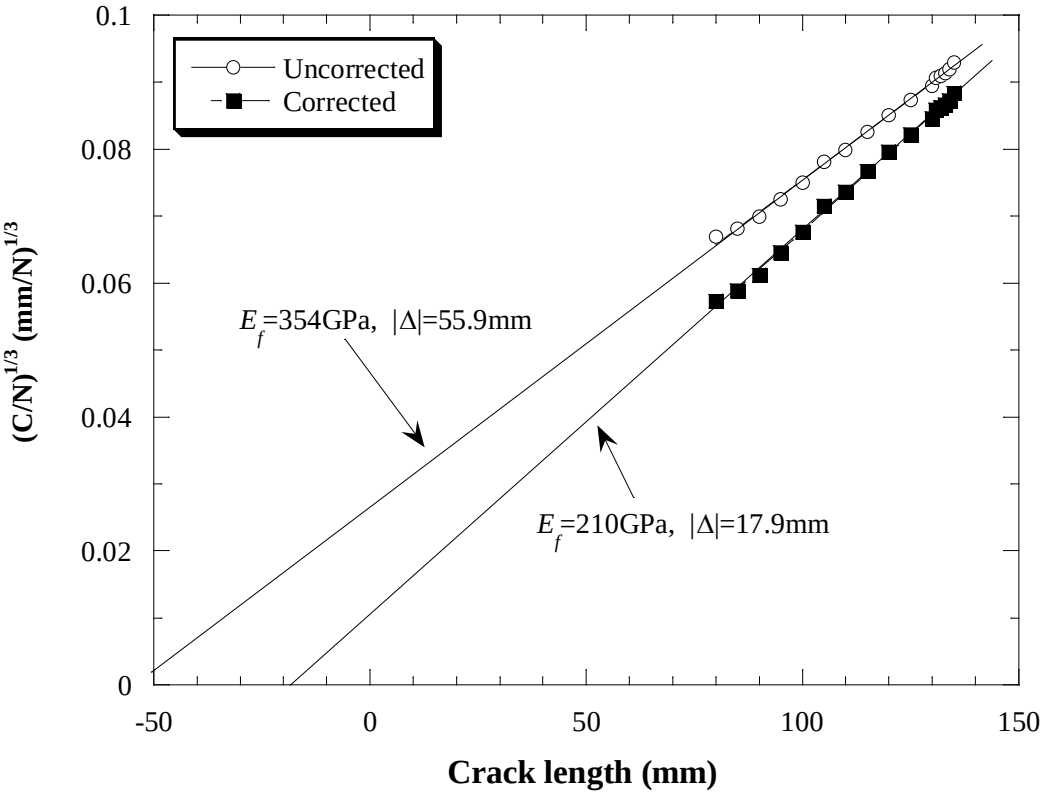

Figure 5. A graph showing the values of $(C/N)^{1/3}$ versus crack length for a typical DCB joint manufactured with mild steel substrates. The effects of applying the system compliance correction to the data are highlighted.

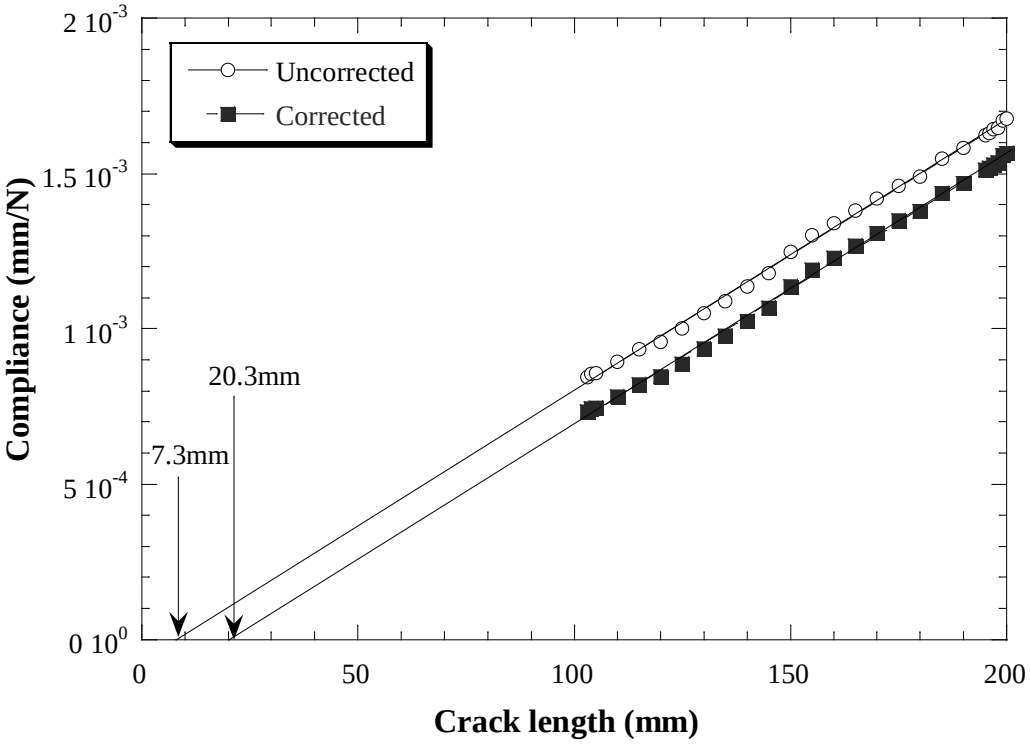

Figure 6. A graph showing the values of the compliance versus crack length for a typical TDCB joint manufactured with aluminium alloy substrates. The effects of applying the system compliance correction to the data are highlighted.

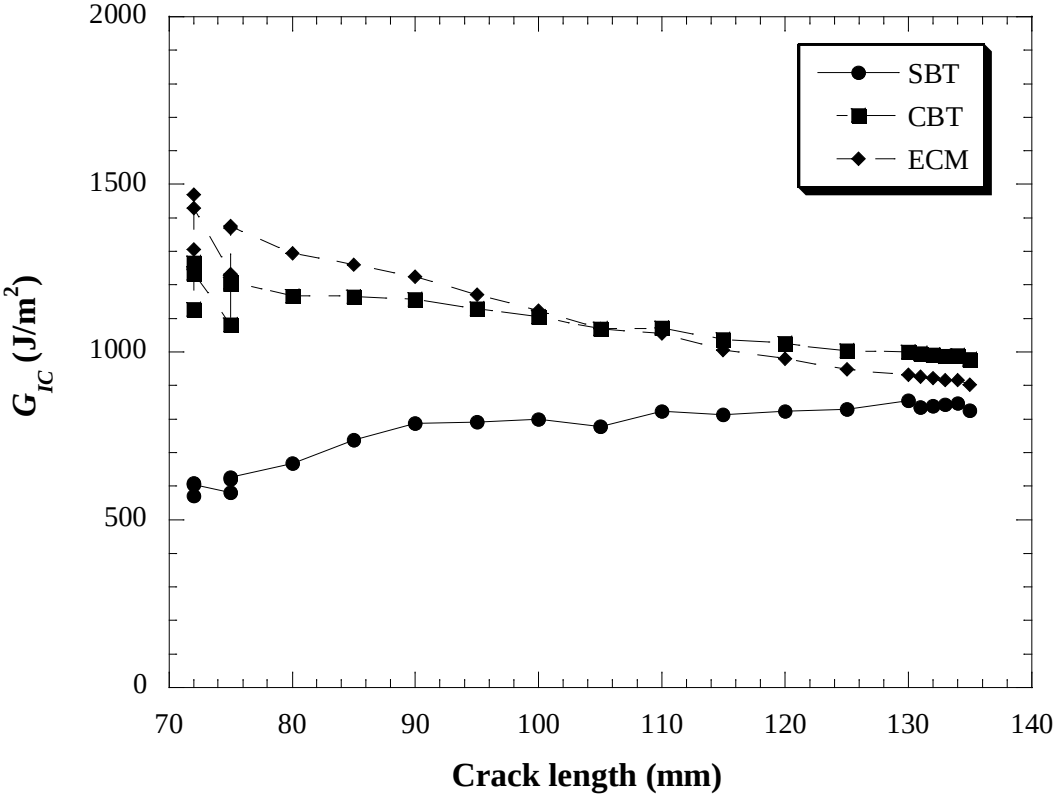

Figure 7(a) A typical set of resistance curves for a DCB joint manufactured with the mild steel substrates and deduced via the three different analysis techniques (SBT, CBT and ECM methods). These data have not been corrected for the effects of system compliance.

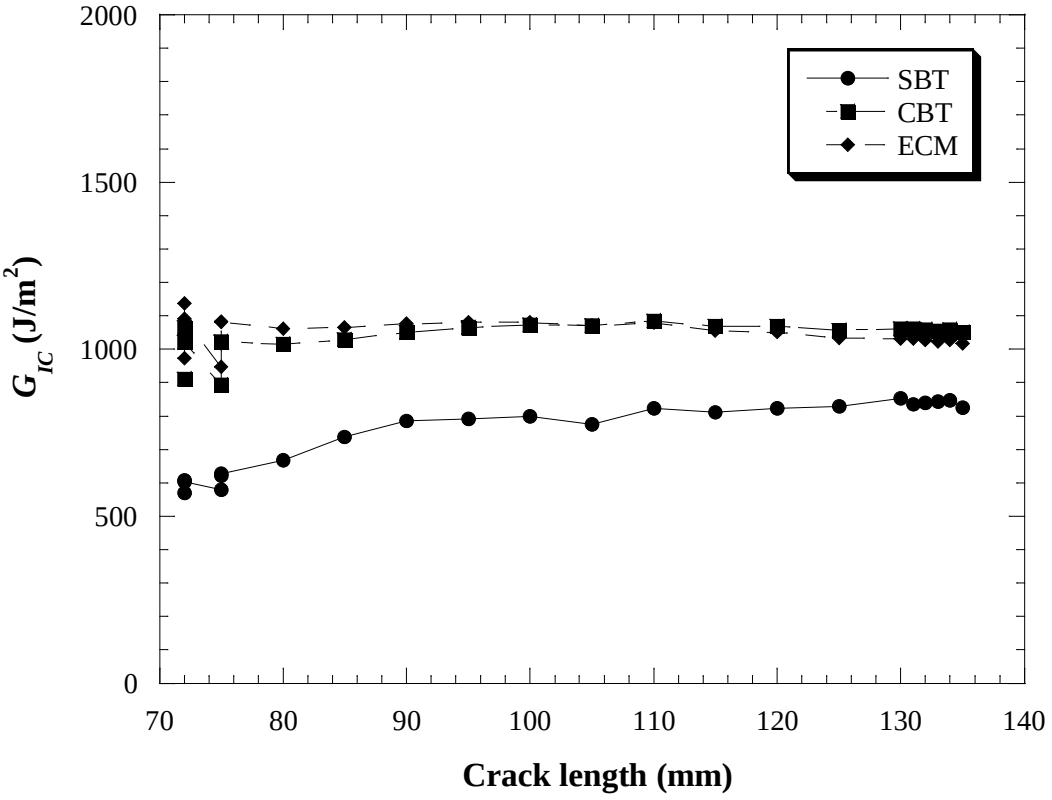

Figure 7(b) A typical set of resistance curves for a DCB joint manufactured with the mild steel substrates and deduced via the three different analysis techniques (SBT, CBT and ECM methods). These data have been corrected for the effects of system compliance.

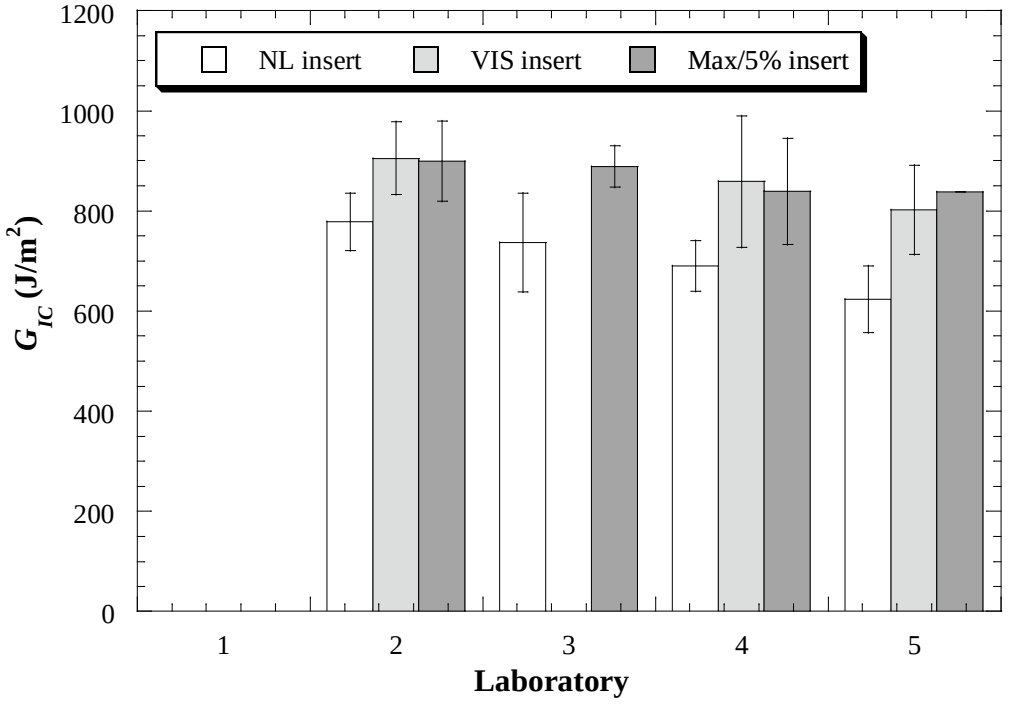

Figure 8(a). Initiation values of G_{IC} measured from the insert for the TDCB joints manufactured with the mild steel substrates as tested by laboratories 1-5. Values of the non-linear (NL), visual (VIS) and (Max/5%) definitions are shown. The height of the columns represent the within laboratory mean values and the error bars represent the within laboratory standard deviations. (Notes: Laboratory 1 did not report any initiation values and Laboratory 3 did not report any visual initiation values).

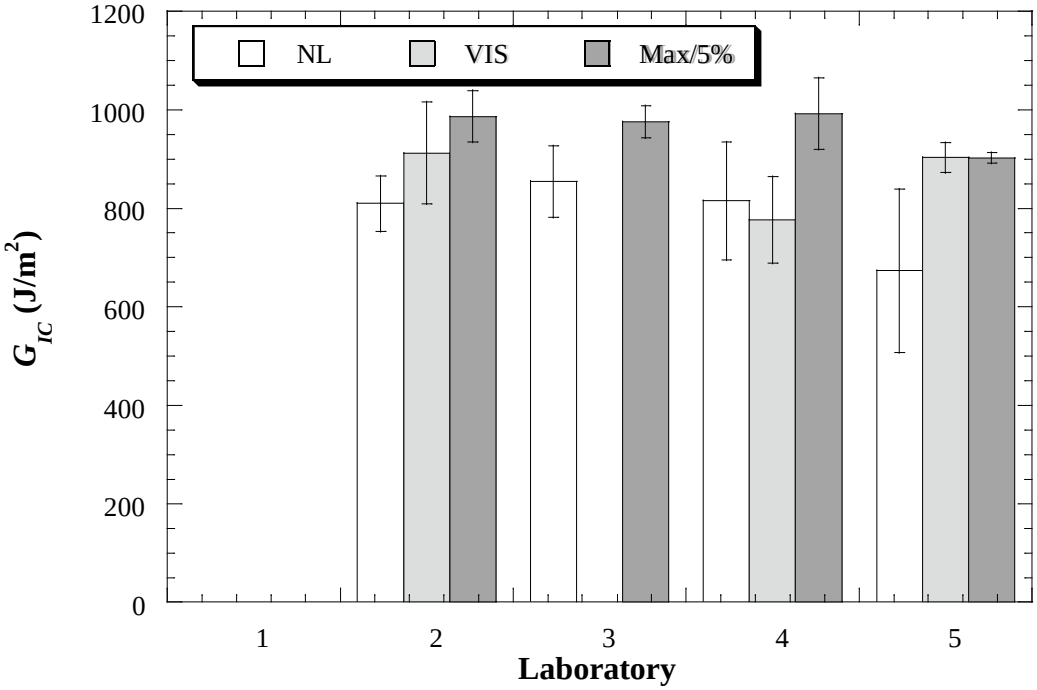

Figure 8(b). Initiation values of G_{IC} measured from the mode I precrack for the TDCB joints manufactured with the mild steel substrates as tested by laboratories 1-5. Values of the non-linear (NL), visual (VIS) and (Max/5%) definitions are shown. The height of the columns represent the within laboratory mean values and the error bars represent the within laboratory standard deviations. (Notes: Laboratory 1 did not report any initiation values and Laboratory 3 did not report any visual initiation values).

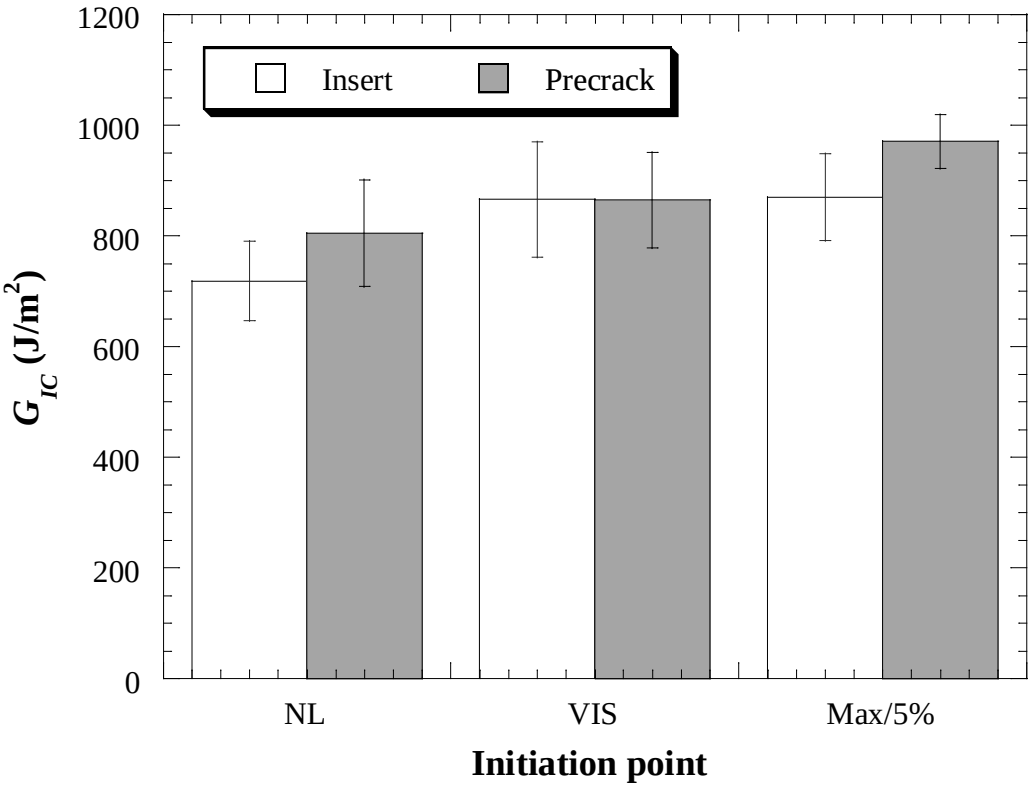

Figure 8(c). Comparison of initiation values of G_{IC} measured from the insert and from the mode I precrack for the TDCB joints manufactured with the mild steel substrates as tested by laboratories 1-5. Values of the non-linear (NL), visual (VIS) and (Max/5%) definitions are shown. The height of columns represent the within laboratory mean values and the error bars represent the repeatability standard deviation *S*r (see precision values).

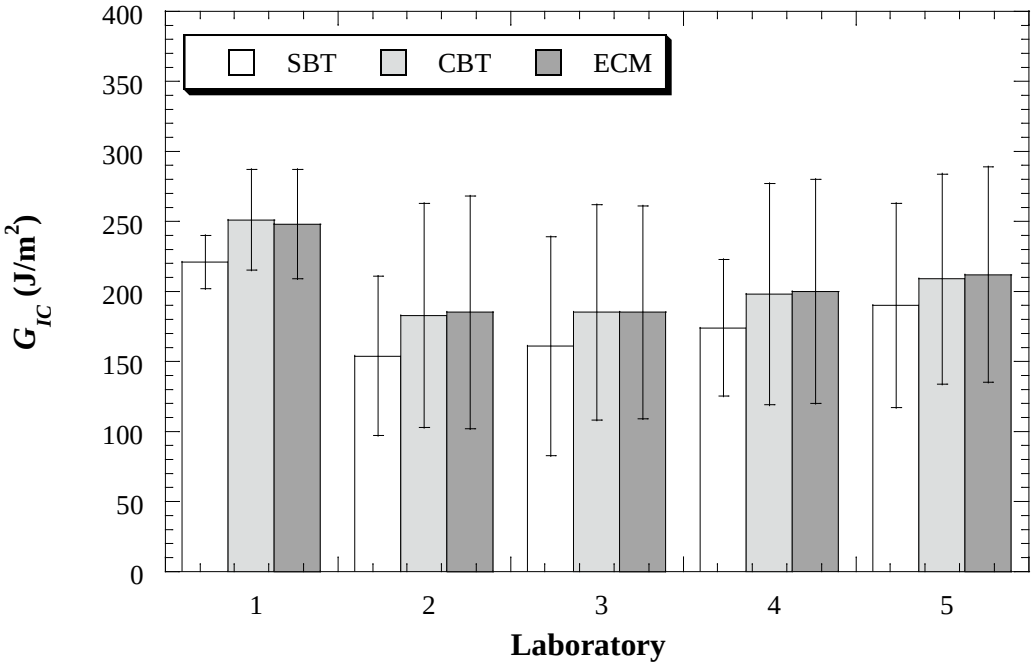

Figure 9. The mean propagation values of G_{IC} for the DCB joints manufactured with the CFRP substrates as tested by laboratories 1-5. The values obtained using the different data reduction methods i.e. SBT, CBT and ECM methods are compared. The height of the columns represent the within laboratory mean values and the error bars represent the within laboratory standard deviations.

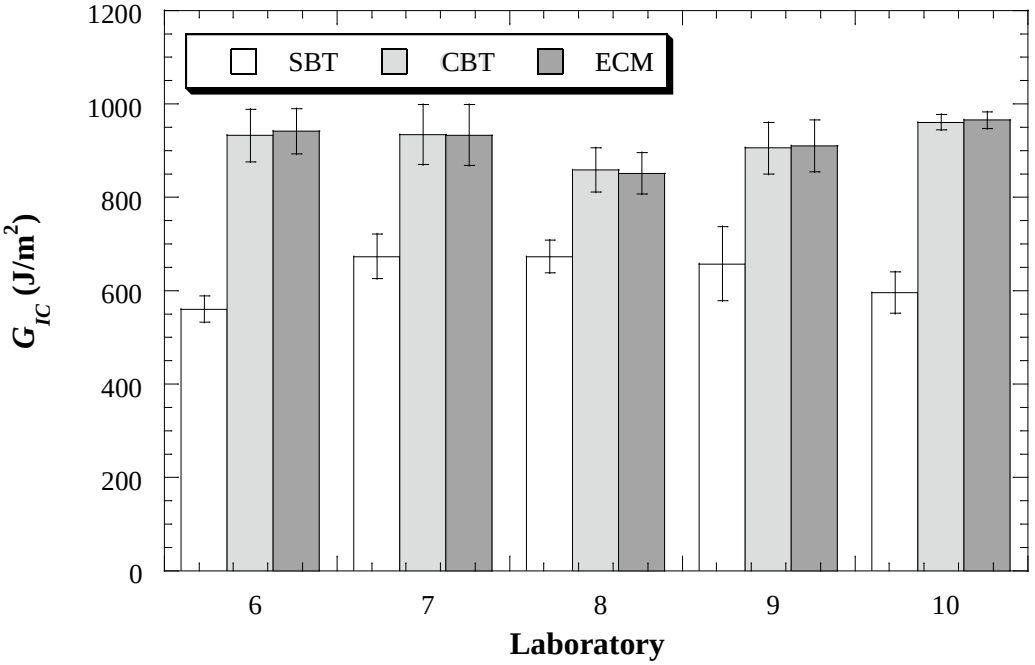

Figure 10. The mean propagation values of G_{IC} for the DCB joints manufactured with the mild steel substrates as tested by laboratories 1-5. The values obtained using the different data reduction methods i.e. SBT, CBT and ECM methods are compared. The height of the columns represent the within laboratory mean values and the error bars represent the within laboratory standard deviations.

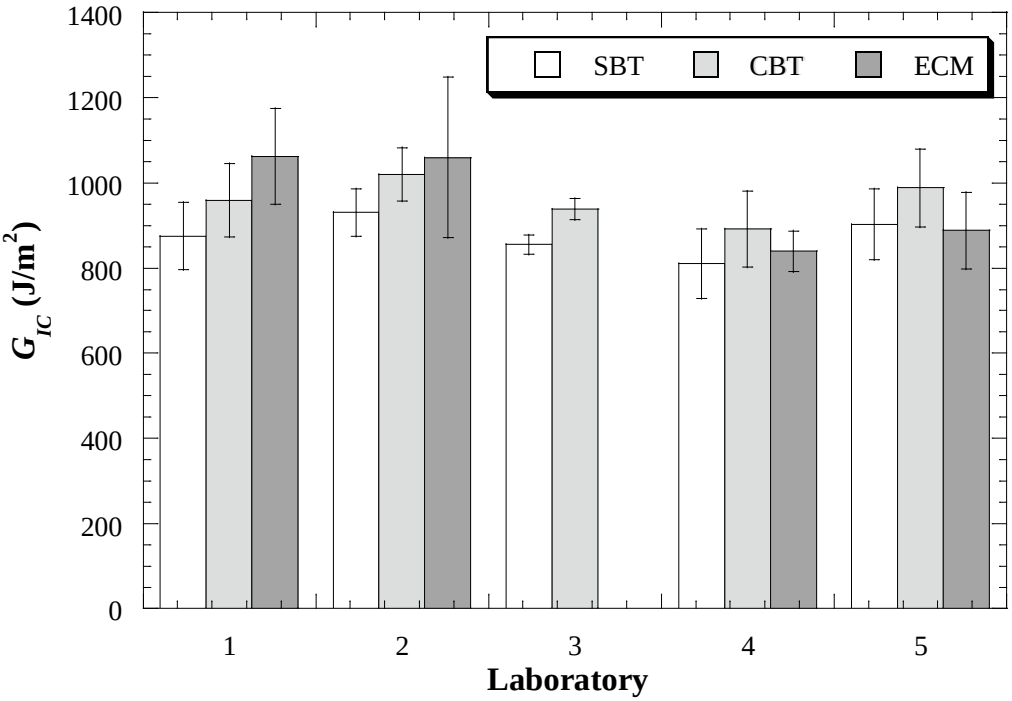

Figure 11. The mean propagation values of G_{IC} for the TDCB joints manufactured with the mild steel substrates as tested by laboratories 1-5. The values obtained using the different data reduction methods i.e. SBT, CBT and ECM methods are compared. The height of the columns represent the within laboratory mean values and the error bars represent the within laboratory standard deviations. (Note: Laboratory 3 ECM data was identified as outlying and was discarded).

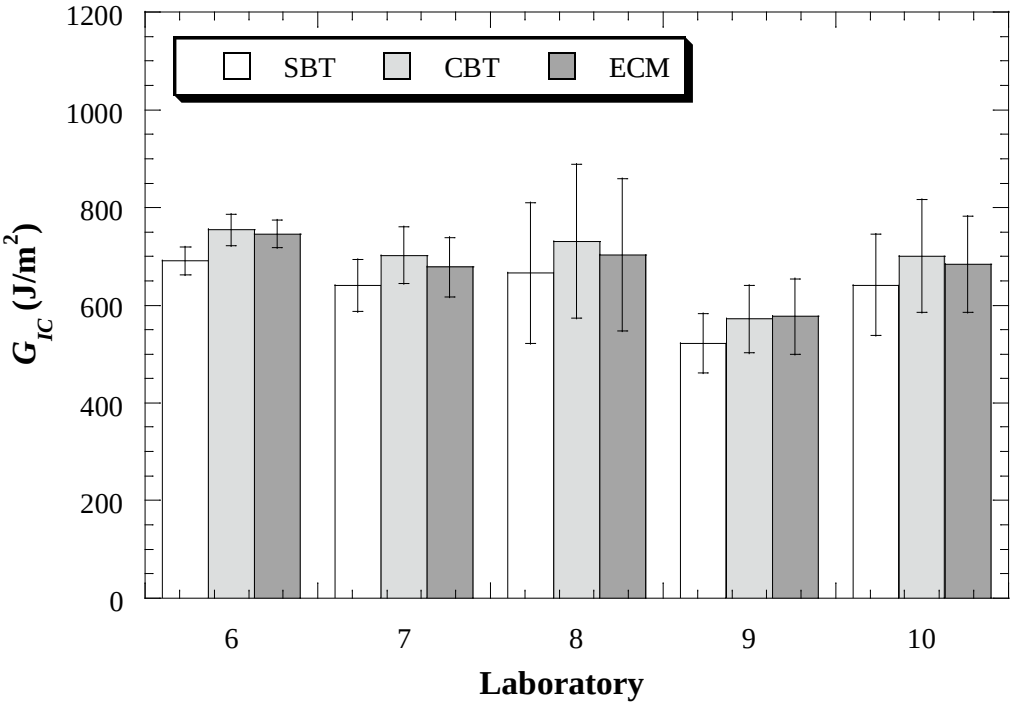

Figure 12. The mean propagation values of G_{IC} for the TDCB joints manufactured with the aluminium alloy substrates as tested by laboratories 6-10. The values obtained using the different data reduction methods i.e. SBT, CBT and ECM methods are compared. The height of the columns represent the within laboratory mean values and the error bars represent the within laboratory standard deviations.

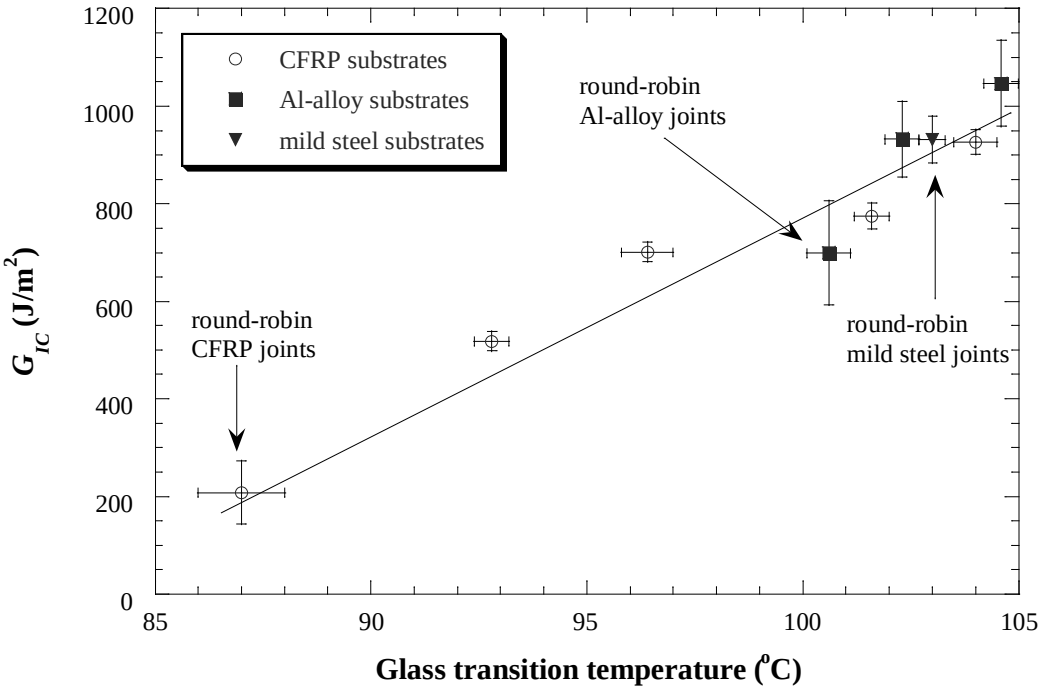

Figure 13. The correlation between the adhesive fracture energy, G_{IC}, and the glass transition temperature, T_g , of the cured adhesive. The joints tested in the round-robin are highlighted. The other data were measured in a later study [20].